Simultaneous increase in conductivity and phonon scattering in a graphene nanosheets/$(Bi_2Te_3)_{0.2}(Sb_2Te_3)_{0.8}$ thermoelectric nanocomposite

Cong Li, Xiaoying Qin[*], Yuanyue Li, Di Li, Jian Zhang, Haifeng Guo, Hongxing Xin, Chunjun Song

Key Laboratory of Materials Physics, Institute of Solid State Physics, Chinese Academy of Science, 230031 Hefei, PR China

A R T I C L E   I N F O

A B S T R A C T

A thermoelectric nanocomposite of $Bi_{0.4}Sb_{1.6}Te_3$ (BiSbTe) incorporated with the graphene nanosheets (GNs) has been synthesized and studied. The reduction of the carrier mobility is much less than the increase of the carrier concentration, resulting in the increase in conductivity at a low graphene nanosheets content. Simultaneously, graphene nanosheets causes 20—30% reduction in thermal conductivity (κ) owing to phonons blocking of nanosheets as well as phase boundaries. As a result, high dimensionless figure of merit (ZT) values of up to 1.29 (300 K) and 1.54 (440 K) are obtained in $Bi_{0.4}Sb_{1.6}Te_3$ incorporated with only 0.3 vol.% and 0.4 vol.% graphene nanosheets, respectively, demonstrating that the thermoelectric performance of the BiSbTe alloy can be improved effectively through incorporation of GNs.

1. Introduction

Thermoelectric (TE) materials have captured extensive attention because of their potential use in direct thermal-to-electrical energy conversion and solid-state refrigeration. The performance of a thermoelectric material can be quantified by the dimensionless figure of merit $ZT = S^2T/\rho(\kappa_c + \kappa_L)$, where S is the Seebeck coefficient, ρ is the electrical resistivity, T is the operating temperature, κ_c is the electronic thermal conductivity and κ_L is the lattice thermal conductivity, respectively [1,2]. It is clear that there are usually two ways to improve ZT: one is to boost the power factor PF (S^2/ρ) and the other is to reduce thermal conductivity (κ).

Previous studies and recent advances in theories and experiments have confirmed that the scattering of long and mid-wavelength phonons can substantially enhance the ZT by employing a high density of nanometer-sized grain boundaries [3]. Using a variational method, Bergman et al. showed that the effective dimensionless figure of merit (ZT) of composite TE materials could not exceed the largest ZT of its constituents [4] unless there is size or interfacial effects [5]. For example, one can reduce the thermal conductivity and thus increase the ZT of PbTe by forming

nano inclusions during solid-state synthesis to enhance phonon scattering at the interface between the matrix and the inclusion [6]. Another means is to introduce secondary (usually non-thermoelectric) phases via powder processing, such as adding C_{60} into bismuth telluride-based materials [7—9], C_{60} into skutterudites [10,11] single-walled carbon nanotube (CNT) into Bi_2Te_3 [12].

Bi_2Te_3-based alloys are the state-of-the-art thermoelectric materials that are (uniquely) used commercially at near room temperature for refrigeration. Numerous researches have been performed to enhance their ZT by structural and composition modification since Bi_2Te_3-based alloys were found in 1960s [13—20]. Recently, the Bi_2Te_3-based nanostructured thermoelectric materials have been investigated to achieve enhanced ZT by reducing thermal conductivity κ [21—27].

Graphene, another special form of carbon except for CNT and C_{60}, in which the atoms form a flat sheet just one atom thick, has attracted a great deal of attention in recent years because of its strictly 2D structure and its unique electrical, optical, catalytic and mechanical properties. Du et al. [28] have reported that graphene nanosheets (GNs) exhibit high electrical conductivity at room temperature due to their very high electron mobility in a polyaniline/graphene nanosheets thermoelectric nanocomposite.

In our present study, we synthesized and studied the thermoelectric nano composite of $(Bi_2Te_3)_{0.2}(Sb_2Te_3)_{0.8}$ incorporated with graphene nanosheets (GNs/$Bi_{0.4}Sb_{1.6}Te_3$), wanting to enhance its ZT

by taking advantage of the unique carbon nanostructures of graphene nanosheets. Our experimental results indicate that the dispersion of graphene nanosheets in BiSbTe can indeed elevate PF by changing carrier mobility and carrier concentration and reduce lattice thermal conductivity via phonon scattering by the nano-inclusion, leading to substantial enhancement of its ZT near room temperature.

2. Experimental

2.1. Preparation procedure

Elemental powders Bi (99.99%, Alfa Aesar), Sb (99.5%, Sigma Aldrich), and Te (99.5%, Alfa Aesar) granules were weighted according to the formula of $(Bi_2Te_3)_{0.2}(Sb_2Te_3)_{0.8}$ doped with 3 wt.% Te. The powder mixture was loaded into quartz ampoule sealed under vacuum at 10^{-3} Pa, and then heated to 1073 K for 10 h. Then the ingot was grinded into powders. 2 g of dried graphite comprising hundreds of carbon layers were dispersed in 300 ml of acetone (AR) by a mechanical stirring, introduced with zirconia balls into a ceramic pot, and milled in a planetary mill at a mild rotation speed 180 r.p.m. to ensure the shear stress is dominant. After 10 h of the shear-force-dominated grinding, the obtained dark dispersion was placed still in order to let large pieces subside completely, and then was subjected to centrifugation at 4000 r.p.m. for 5 min to remove any macroscopic aggregates using a TGL-10B centrifuge, giving a light black suspension where single- and few-layer graphene sheets were readily prepared and suspended homogeneously and stably in the acetone medium. $(Bi_2Te_3)_{0.2}(Sb_2Te_3)_{0.8}$ powders were blended into the colloidal dispersions of graphene nanosheets in the acetone solvent, heating and magnetic stirring in water bath until giving the dried powders. With this, a series of f(GNs)/BiSbTe nanocomposites with certain volume fraction (f = 0, 0.1, 0.2, 0.3 and 0.4 vol.%) have been prepared.

Dried powders of GNs/$(Bi_2Te_3)_{0.2}(Sb_2Te_3)_{0.8}$ nanocomposite were hot-pressed under vacuum at 10^{-2} Pa into dense pellets at a pressure of 600 MPa at 350 °C for 1 h, obtaining compacted bulk materials. Bars of about $1.5 \times 3 \times 10$ mm were cut from the pressed disks and polished for the thermoelectric properties characterization. The electrical resistivity and the Seebeck coefficient were measured simultaneously by commercial equipment (ULVAC-RIKO: ZEM-3, Japan) under He atmosphere from 293 to 498 K. The thermal diffusivity, α, was measured using the laser flash method (Netzsch, LFA 457). The specific heat, Cp, was determined by a commercial instrument (Pyris Diamond DSC, Perkine Elmer). The density, D, was measured by the Archimedes' method (using ethyl alcohol as liquid medium, AR). The resulting total thermal conductivity was calculated from the measured thermal diffusivity α, density D and specific heat Cp from the relationship $\kappa = \alpha DCp$. The Hall coefficient was measured at 300 K using the physical property measurement system (PPMS), and the carrier concentrations and mobility were calculated using Hall coefficient and electrical resistivity.

2.2. Characterization

Microstructure analysis of the prepared graphene sheets using high resolution transmission electron microscopy (HRTEM, JEOL JEM-2010) was performed. The phase structure of sample was studied by X-ray diffraction (XRD, Philips diffractometer, Cu Ka radiation) at room temperature. The fractograph of the composite f(GNs)/BiSbTe (Here, we take f = 0.2 vol.% for instance.) were observed by field emission scanning electron microscopy (FE-SEM, FEI Sirion 200) and Raman spectroscopy (RS, Renishaw inVia Reflex,

LAICA DM2500).

3. Results and discussion

3.1. Microstructural characterization

As shown in Fig. 1 ((a)and(b)), single- and few-layer graphene sheets were prepared. Typically flat sheets show a lateral size about 100–200 nm. Meanwhile, the graphene sheets have a significant tendency to coalesce into overlapped structures and are somewhat wrinkled on the grid to form graphitic structures due to the high surface area.

The XRD patterns of composite f(GNs)/BiSbTe (f = 0, 0.1, 0.2, 0.3 and 0.4 vol. %) are shown in Fig. 2. All the main diffraction peaks match well with the standard JCPDS (PDF#01-072-1836) card of $Bi_{0.4}Sb_{1.6}Te_3$ with rhombohedral structure (crystal group R3m). As compared with the pattern of BiSbTe, no obvious changes are detected in XRD patterns for f(GNs)/BiSbTe composites sample, but graphene nanosheets' existence was confirmed by RS as shown later.

Fig. 3 shows the FE-SEM fractographs of the sintered bulk composite samples. Because of the low sintering temperature and fast sintering process, fine-grained microstructure can be expected. As shown in the field emission scanning electron microscopy (FE-SEM) image (Fig. 3), a lot of plate-shaped grains can be observed, which are characteristics of the layer structure of Bi_2Te_3-based compounds. Meanwhile, one can hardly find the existence of graphene nanosheet from the FE-SEM owing to its low content and its unique carbon structure.

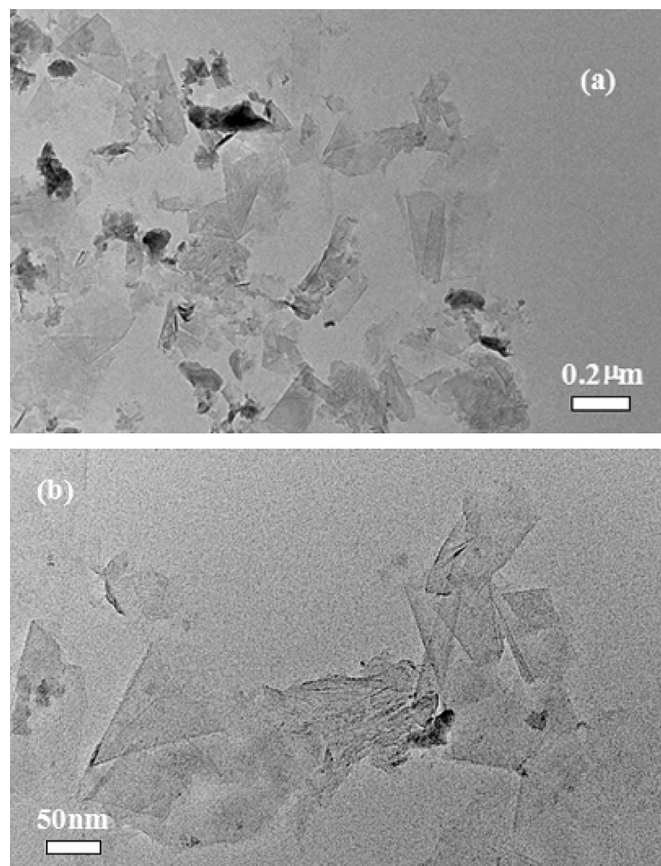Raman measurements were conducted on several spots of the

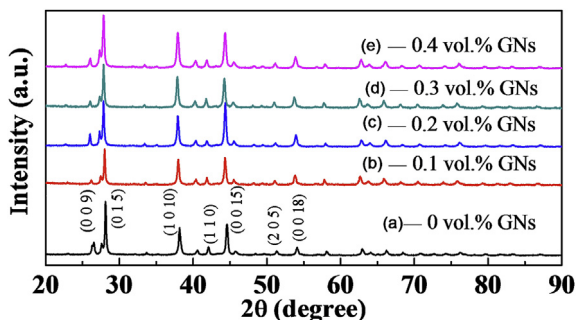**Fig. 1.** HRTEM image of graphene sheets from the acetone supernatant.

Fig. 2. XRD patterns of *f*(GNs)/BiSbTe: (a) *f* = 0, (b) *f* = 0.1, (c) *f* = 0.2, (d) *f* = 0.3 and (e) *f* = 0.4 vol. % at room temperature.
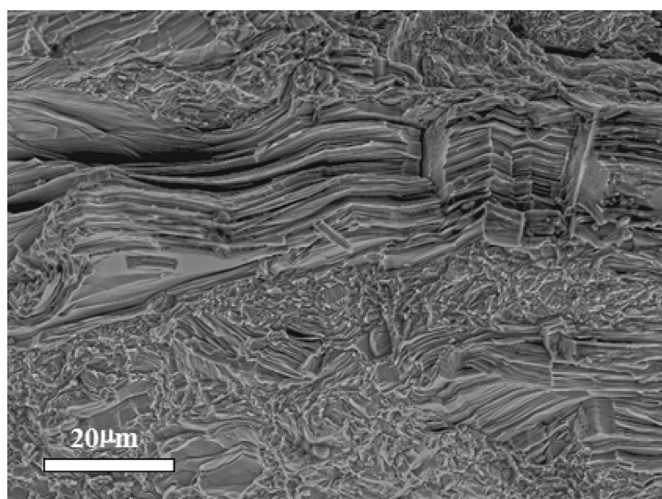

Fig. 3. FE-SEM fractographs of *f*(GNs)/BiSbTe sample at room temperature.

Fig. 4. (a) Room-temperature Raman spectra of the fractograph of *f*(GNs)/BiSbTe (*f* = 0.2 vol. %); (b) Raman mapping for I_G (the intensity of the G peak, 1580 cm^{-1}) of the fractograph of *f*(GNs)/BiSbTe (*f* = 0.2 vol. %) at room temperature.

fractograph of the as-prepared *f*(GNs)/BiSbTe (*f* = 0.2 vol.%) composite. Similar Raman spectra, showing a D peak at 1350 cm^{-1}, a G peak at 1580 cm^{-1}, a 2D peak at 2700 cm^{-1} (Fig. 4 (a)), were obtained, matching well with the previously reported data from graphenes [29]. This obviously suggests that the crystal structure of graphene had been preserved satisfactorily and incorporated successfully into BiSbTe matrix. Moreover, as shown in the Raman mapping (Fig. 4 (b)), the GNs was detected in spite of its weak signal. Graphene nanosheets are located at the red circled areas, and it further confirmed that the graphene nanosheets are homogeneously distributed throughout the sample although its volume fraction is as low as 0.2 vol.%.

3.2. Thermoelectric properties

All five *f*(GNs)/BiSbTe (*f* = 0, 0.1, 0.2, 0.3 and 0.4 vol.%) composites sample exhibited similar trends in electrical and thermal-transport properties between 300 K and 498 K (Figs. 5–9).

Temperature dependence of electrical resistivity ρ was shown in Fig. 5(a). The electrical resistivity increases monotonically with the increasing temperature, showing the characteristics of degenerate semiconducting behavior. In general, ρ increased lightly with increasing GNs content, as an example, ρ increases from 0.71 × 10^{-3} Ω cm, to 0.75 × 10^{-3} Ω cm, to 0.76 × 10^{-3} Ω cm and 0.77 × 10^{-3} Ω cm at 300 K with *f* increases from 0 vol.%, to 0.1 vol.%, to 0.2 vol.% and 0.4 vol.%, respectively. What is noteworthy is that in the case of addition *f* = 0.3 vol.%, the electrical resistivity decreases
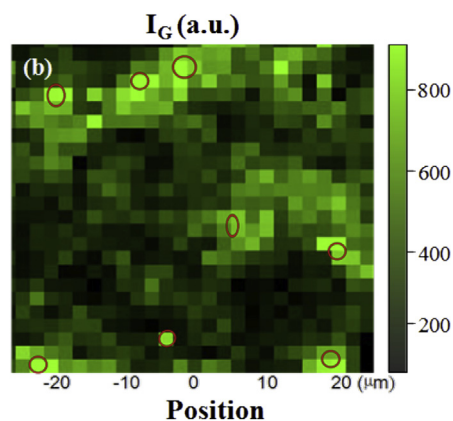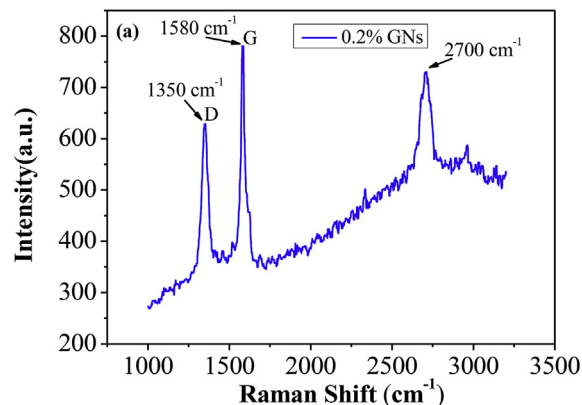
specially at high temperature (480 K, for instance) as compared to that of the matrix BiSbTe. Moreover, it is found that the slopes (dρ/dT) of the ρ-T curve for sample (*f* = 0.3 vol.%) is smaller than that of other samples, which could involve a significant scattering mechanism (see following discussion).

Fig. 5(b) demonstrates Seebeck coefficient for *f*(GNs)/BiSbTe (*f* = 0, 0.1, 0.2, 0.3, 0.4 vol.%). The positive values of the S mean that the major charge carriers in all the samples are holes. In addition, the Seebeck coefficient for the nanocomposite samples was observed to increase with increasing temperature, and after reaching a maximum value, it showed a slight decrease obviously with further increase in temperature. This behavior has been reported previously [30] and could be attributed to thermal excitation of minority carriers at high temperature. Moreover, S generally decreases lightly with increasing GNs content below~370 K. Specially, for instance, S for 0.1 vol.%, 0.2 vol.%, 0.3 vol.%, 0.4 vol.% GNs/BiSbTe composite sample at 300 K reaches 178 μV/K, 174 μV/K, 177 μV/K, 173 μV/K, respectively, which is a little lower than that (179 μV/K) of the BiSbTe matrix.

Since the electrical resistivity and the Seebeck coefficient strongly depend on carrier concentration, their changes can be well explained by the variation of the carrier concentration p. The electrical resistivity (ρ) and Seebeck coefficient (S) can be expressed in terms of the carrier concentration (p) by the Mott equation, as follows:
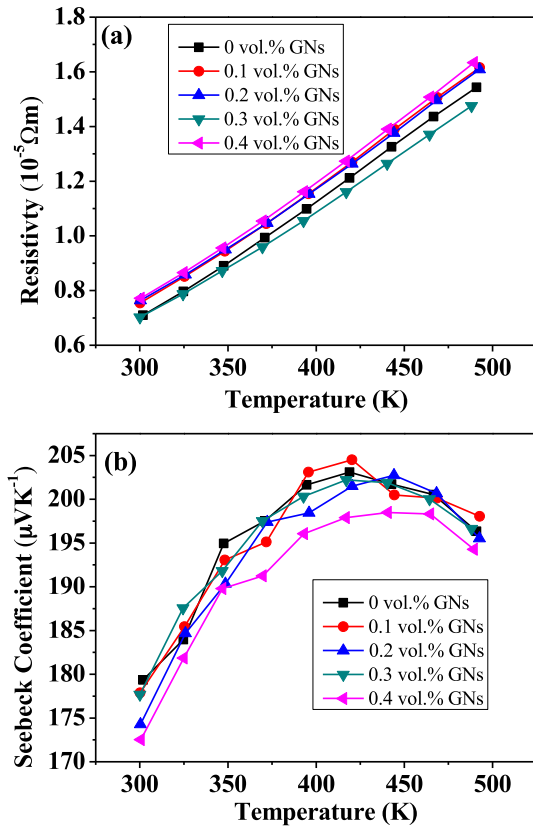
$$\rho = \frac{1}{p\mu q} \tag{1}$$

Fig. 5. Temperature dependence of (a) electrical resistivity (ρ), (b) Seebeck coefficient (S) for f(GNs)/BiSbTe (f = 0, 0.1, 0.2, 0.3 and 0.4 vol.%) samples.

$$S = \frac{\pi^2 k_B^2 T}{3q}\left[\frac{\partial \ln(\partial(E))}{\partial E}\right]_{E=E_f}$$

$$= \frac{\pi^2 k_B^2 T}{3q}\left[\frac{1}{p}\frac{\partial p(E)}{\partial E} + \frac{1}{\mu}\frac{\partial \mu(E)}{\partial E}\right]_{E=E_f} \qquad (2)$$

where p, μ, q, k_B, σ and E_f are carrier concentration, carrier mobility, carrier charge, Boltzmann constant, electrical conductivity and Fermi energy, respectively.

Hall coefficient measurement indicates that as f increases the carrier concentrations p increases substantially in a tolerant error range, as given in Table 1. According to the Mott equation (formula (2)), one can find that the decrease in S is caused by the increase in

p. Previous studies [31] indicate the holes (carrier) are generally created by the antistructure defects, and, the increase in carrier (holes) concentration (p) for all the composite samples probably because more antistructure defects are formed with increasing GNs content. Simultaneously, the carrier mobility μ declines from 290.9 cm^2 V^{-1} s^{-1} to 233.2 cm^2 V^{-1} s^{-1}, 207.4 cm^2 V^{-1} s^{-1} and 208.5 cm^2 V^{-1} s^{-1} with increasing f, due to enhanced interface scattering. It is worth pointing out that p and μ for f(GNs)/BiSbTe (f = 0.3 vol.%) is 3.71 × 10^{19} cm^{-3} and 240.6 cm^2 V^{-1} s^{-1}. The reduction of the carrier concentration is much less than the carrier mobility increase, therefore, it is clear now that the increase of σ for f(GNs)/BiSbTe (f = 0.3 vol.%) is totally caused by the substantial increase in carrier concentration (p) and boosted carrier mobility (μ) compared to other composite samples.

As mentioned above, in the case of addition f = 0.3 vol.%, the electrical resistivity decreases as compared to that of the matrix BiSbTe. Here, we assume that p does not change substantially (which is true for a degenerate semiconductor at the temperatures below intrinsic excitation [32,33]) in the temperature range (300 K < T < 450 K) investigated here. Then the total carrier mobility ($μ_T$) can be estimated from values of ρ at different temperatures, as given in Fig. 6(a). If we assume that the scattering events are independent with each other, then one has [34]:

$$\frac{1}{\mu_T} = \frac{1}{\mu_m} + \frac{1}{\mu_{in}} \qquad (3)$$

where $μ_T$, $μ_m$ and $μ_{in}$ are the total carrier mobility of the composite samples, the mobility of the matrix and the mobility being related to scattering of interface potentials. Based on the experimental data, one can extract $μ_{in}$ by using formula (3), as shown in Fig. 6(b). Obviously, $μ_{in}$ for f(GNs)/BiSbTe (f = 0.3 vol.%) is much bigger than other composite samples (f = 0.1, 0.2 and 0.4 vol.%) caused by interface scattering, which alleviates the decline rate in total carrier mobility ($μ_T$), resulting in a lower electrical resistivity.

Similar to the scattering of grain boundary potentials, $μ_{in}$ caused by interface scattering in nanocomposites can be approximately given by Refs. [35,36]:

$$\mu_{in} = Lq\left(\frac{1}{2\pi m_d^* k_B T}\right)^{1/2} \exp\left(-\frac{E_B}{k_B T}\right) \qquad (4)$$

where L is the mean spacing between two adjacent potential barriers, and E_B is the height of the potentials at the interfaces. A logarithmic plot of $μ_{in}$ × $T^{1/2}$ versus 1/T (here, we take f(GNs)/BiSbTe (f = 0.4 vol.%) composite sample for instance) is shown in Fig. 6(c). From the slope, the height of the potentials is extracted to be E_B = −23.4 meV, showing an apparent interfacial potential well.

Table 1
List of Hall coefficient R_h, carrier concentrations p, Hall mobility μ, the relative density D_r, the Lorenz number L and the volume fraction of phase boundaries F_p for f(GNs)/BiSbTe composite samples with different GNs content f at 300 K.

f	R_h[a] (10^4 cm^3 C^{-1})	p[b] (10^{19} cm^{-3})	μ[c] (cm^2 V^{-1} s^{-1})	D_r (%)[d]	L[e] (10^{-8} V^2 K^{-2})	F_p[f] (10^6 m^2/m^3)
0 vol.%	2.07	3.03	290.9	98.0	1.67	0
0.1 vol.%	1.75	3.57	233.2	97.6	1.70	2.1
0.2 vol.%	1.58	3.97	207.4	97.1	1.72	4.2
0.3 vol.%	1.68	3.71	240.6	96.7	1.70	6.3
0.4 vol.%	1.61	3.89	208.5	96.6	1.71	8.4

[a] R_h is Hall coefficient.
[b] p is carrier concentrations.
[c] μ is Hall mobility.
[d] D_r is the relative density, defined as $D_r = D/D_0$, where D is measured density and D_0 (=6.76 g/cm³) is theoretical density of BiSbTe. For composite samples f(GNs)/BiSbTe, its theoretical density is modified as: $D_0 = (1 - f)D_1 + fD_2$, here $D_1 = D_0$ for BiSbTe and D_2 (=1.06 g/cm³) is theoretical density of graphene.
[e] L is the Lorenz number.
[f] Fp is the volume fraction of phase boundaries.

Fig. 7. Temperature dependence of power factor (PF) for f(GNs)/BiSbTe (f = 0, 0.1, 0.2, 0.3 and 0.4 vol.%) samples.

instance, PF decreases form 45×10^{-4} W m^{-1} K^{-2}, to 42×10^{-4} W m^{-1} K^{-2}, to 40×10^{-4} W m^{-1} K^{-2}, and 38×10^{-4} W m^{-1} K^{-2} at 300 K with f increases from 0 vol.%, to 0.1 vol.%, to 0.2 vol.% and 0.4 vol.%. The slight decrease in PF mainly comes from the increase in ρ. It is noted that the PF value for the composite sample of f = 0.3 vol.% increases compared to that of the matrix BiSbTe, and the maximum value of PF reached 46×10^{-4} W m^{-1} K^{-2} at 300 K. This behavior can be well explained from the changing trend of electrical resistivity ρ.

One can see from Fig. 8 (a) the temperature behavior of the total thermal conductivity for the five samples is similar: it decreases with increasing temperature and then increases with further increasing temperature. What's more, κ for all the composite samples is smaller than that of the BiSbTe matrix and decreases with increasing f in the whole temperate range. Specially, κ for 0.4% GNs/BiSbTe is reduced to 1.04 W K^{-1} m^{-1} at 300 K, to 0.81 W K^{-1} m^{-1} at 490 K, which is about 20% and 28% lower than that (1.25 W K^{-1} m^{-1} and 1.04 W K^{-1} m^{-1}) of the BiSbTe matrix. The total thermal conductivity consists of a phononic contribution κ$_L$ and a contribution of mobile charge carriers, κ$_C$, i.e. κ = κ$_L$ + κ$_C$. Usually, κ$_C$ can be estimated by the Wiedemann-Franzlaw, which relates κ$_C$ to the electrical resistivity ρ according to κ$_C$ = LT/ρ, where L is the Lorentz number, T is the temperature in Kelvin. To determine the electronic component of the thermal conductivity, the Lorenz number L was estimated using formula (5) with the assumption of transport dominated by acoustic scattering and a single parabolic band [37].

$$L = \left(\frac{K_B}{q}\right)^2 \frac{3F_0(\xi_F)F_2(\xi_F) - 4F_1(\xi_F)^2}{F_0(\xi_F)^2} \tag{5}$$

with the Fermi integral of order i,

$$F_i(\xi_F) = \int_0^8 \frac{x^i}{1 + e^{(x-\xi_F)}} dx \tag{6}$$

Here ξ_F is the reduced Fermi level (E$_f$/k$_B$T). The obtained values of L are 1.67–1.72 $\times 10^{-8}$ V^2 K^{-2}, as listed in Table 1. Therefore, κ$_L$ can be obtained by subtracting κ$_C$. As shown in Fig. 8 (b), κ$_L$ in the whole temperature range investigated decreases substantially with increasing f. According to the Callaway mode, the lattice thermal conductivity κ$_L$ can be expressed as [38]:
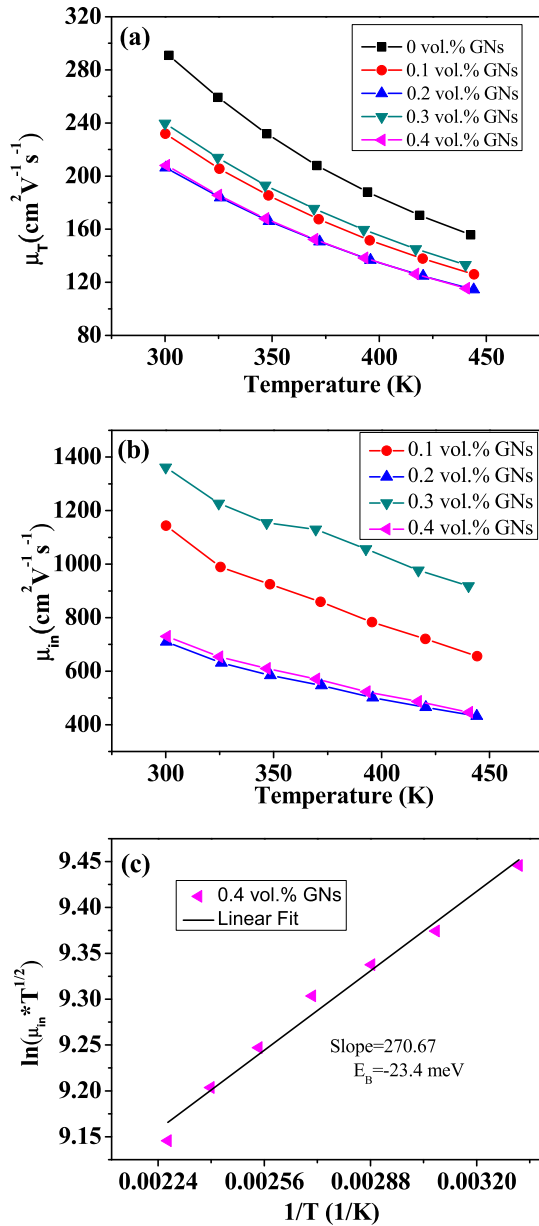

Fig. 6. Temperature dependence of (a) total carrier mobility μ$_T$ and (b) carrier mobility that correspond to the scattering of carriers at the interfaces μ$_{in}$ for composite samples f(GNs)/BiSbTe (f = 0, 0.1, 0.2, 0.3 and 0.4 vol.%); (c) a logarithmic plot of μ$_{in}$*T1/2 versus 1/T (300 K < T < 450 K) for composite samples f (GNs)/BiSbTe (f = 0.4 vol.%).

In the same way, E$_B$ for f(GNs)/BiSbTe (f = 0.1, 0.2 and 0.3 vol.%) was calculated to be −26.8 meV, −23.3 meV and −14.6 meV, respectively. One can see that the absolute value of E$_B$ decreases monotonously with increasing f as f < 0.4 vol.%. The larger |E$_B$| for the sample with f = 0.4 vol.% could be caused by microstructure changes, such as inhomogeneous distribution of the GNs in the BiSbTe matrix due to possible agglomeration at larger GN content (f = 0.4 vol.%). Obviously, the smaller the absolute value of E$_B$ for the sample f(GNs)/BiSbTe(f = 0.3 vol.%) (than that of other composite samples) means that μ$_{in}$ decrease more slowly with increasing temperature based on formula (4), which alleviates the increase rate in ρ of f(GNs)/BiSbTe (f = 0.3 vol.%).

As shown in Fig. 7, power factor (PF) of all the samples decreases with increasing temperature. Also, generally, the PF values of these composite samples decrease with increasing GNs content, for
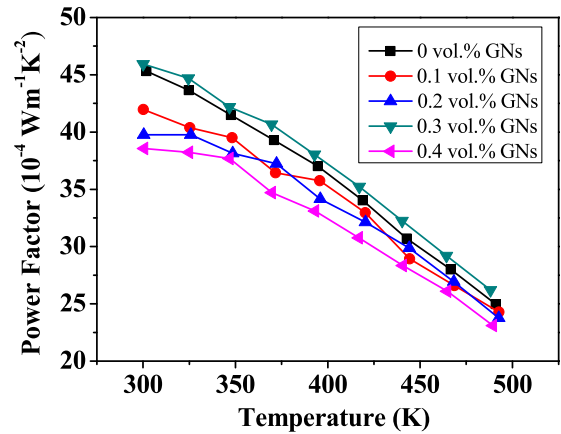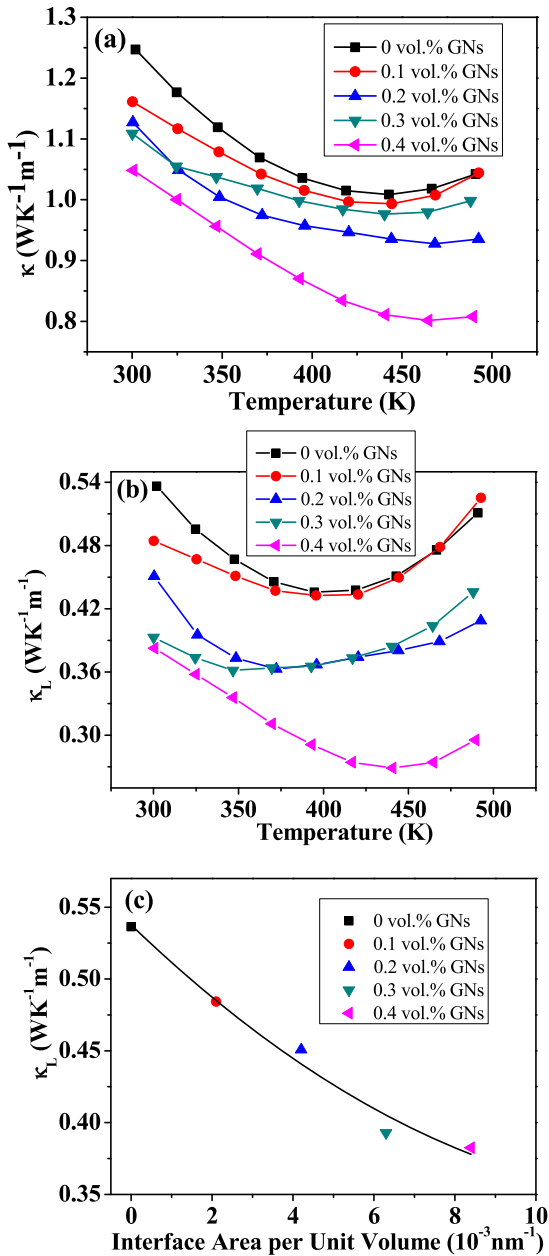
Fig. 8. Temperature dependence of (a) total thermal conductivity (κ), (b) lattice thermal conductivity (κ_L) for f(GNs)/BiSbTe (f = 0, 0.1, 0.2, 0.3 and 0.4 vol.%) samples; (c) lattice thermal conductivity (κ_L) for f(GNs)/BiSbTe (f = 0, 0.1, 0.2, 0.3 and 0.4 vol.%) samples with the volume fraction of phase boundaries F_p at 300 K.

$$k_L = \frac{4\pi k_B^4 T^3}{vh^3} \int_0^{\theta_D} \tau(\xi) \frac{\xi^4 e^\xi}{(e^\xi - 1)^2} dx \quad (7)$$

where h, θ_D, v, ξ and τ are plank constant, Debye temperature, phonon velocity, usual dimensionless variable and phonon relaxation time, respectively. According to Matthiessen's rule, τ is mainly related to scattering from multiple scattering centers in the materials and can be written as:

$$\tau^{-1} = \tau_{PD}^{-1} + \tau_{NP}^{-1} + \tau_{P-P}^{-1} + \tau_{IF}^{-1} \quad (8)$$

where τ_{PD}, τ_{NP}, τ_{p-p} and τ_{IF} are the relaxation times corresponding

to scattering from the point defect, nanoinclusions, phonon–phonon interactions and interfaces, respectively. Obviously, the reduction of κ_L in the composite samples should be attributed to the additional phonon scattering from nanoinclusion (τ_{NP}) and the formed phase boundaries (τ_{IF}).

Previous studies [39] have confirmed that all the interfaces, whether they are grain boundaries or phase boundaries or whether they belong to the coherent or incoherent interfaces, can inhibit the heat flow without exception through phonon scattering in the system, resulting in remarkable reduction in κ_L. Moreover, the studies show that the thermal conductivity depends sensitively on the interface density (interface area per unit volume) following a universal curve. In other words, κ_L reduces gradually with the increasing interface density. Undoubtedly, the volume fraction of phase boundaries F_p (as listed in Table 1) increase with the increasing GNs content for f(GNs)/BiSbTe composites. As shown in Fig. 8(c), it is quite clear that κ_L for f(GNs)/BiSbTe decreases with the increasing F_p, which is originated from the enhanced phonon scattering by the incorporated nanosheets and the phase boundaries. Anomalously, κ for the 0.3 vol.% GNs/BiSbTe composite sample is larger than that of the 0.4 vol.% GNs/BiSbTe sample, which can be attributed to its much higher κ_C caused by the increase in electrical resistivity ρ.

Based on the data obtained above, the temperature dependence of ZT for all the GNs/BiSbTe composite samples is demonstrated in Fig. 9. As seen in Fig. 9, the temperature behavior of ZT for the five samples is similar: it increases with increasing temperature, and after reaching a maximum value ZT decreases with further increasing temperature. For the composite samples with f = 0.1 vol.%, ZT is smaller than that of matrix BiSbTe in the whole temperature range due to smaller PF and a slight decrease in thermal conductivity κ. Nevertheless, ZT of the composite sample with f = 0.2 vol.%, 0.3 vol.% and 0.4 vol.% is obviously larger than that of BiSbTe matrix. Specifically, ZT of the composite samples with f = 0.3 vol.% is substantially larger than that of BiSbTe matrix at T < ~400 K, which is significant since BiSbTe is usually used at near room temperature as refrigeration component. And also, ZT of the composite samples with f = 0.4 vol.% increased remarkably at T > ~400 K, reaching a maximum value of 1.54 at 440 K, which is round 10% larger than that of NC BiSbTe (ZT$_{max}$ = 1.4 at 373 K) [40]. What is worth pointing out is that ZT for all the samples is larger than that of NC BiSbTe at T > ~400 K (as shown in Fig. 9).Clearly, such an excellent thermoelectric performance (at T > ~400 K) could be applied to waste heat recovery utilization. The good thermoelectric properties for the composite samples with f = 0.2 vol.%, 0.3
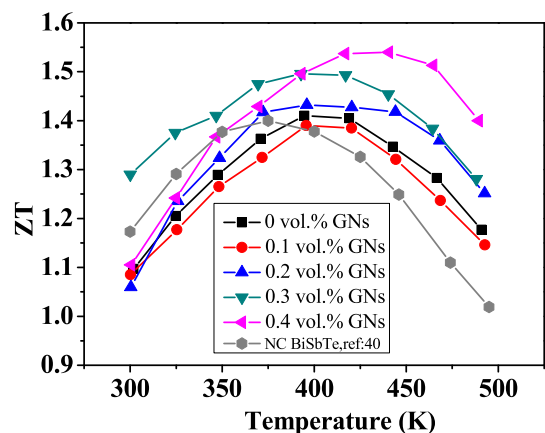

Fig. 9. ZT values with temperature for f(GNs)/BiSbTe composite samples (f = 0, 0.1, 0.2, 0.3 and 0.4 vol.%) and the nanocrystalline BiSbTe bulk sample in Poudel's work.

vol.% and 0.4 vol.% originate from the relatively low thermal conductivity owing to embedded graphene nanosheets though the power factor value has just a little change compared to that of matrix BiSbTe.

4. Conclusions

Composites f(GNs)/BiSbTe (f = 0, 0.1, 0.2, 0.3 and 0.4 vol.%) were prepared, and their thermoelectric properties were studied at temperatures from 300 to 498 K. The results indicate that electrical resistivity for f = 0.3 vol.% decreases due to the obvious changes in carrier concentrations and carrier mobility, meanwhile, Seebeck coefficient decreases slightly at T < ~370 K owing to increase in carrier concentrations. Specially, the incorporation of graphene nanosheets into BiSbTe can significantly reduce the lattice thermal conductivity of BiSbTe, which can be attributed to enhanced phonon scattering by the embedded nanosheets and the phase boundaries. As a result, ZT of f(GNs)/BiSbTe with f = 0.3 vol.% reaches 1.29 at 300 K (which is larger than that (1.09) of BiSbTe matrix in the present study), and specially its maximum ZT for f = 0.4 vol.% reaches 1.54 at 440 K, which is round 15% larger than that (1.34) of BiSbTe matrix. Present results suggest that incorporation of graphene nanosheets into thermoelectric materials, such as BiSbTe-based alloys, could be an effective way to enhancing their thermoelectric performance.

Acknowledgments

References

[1] T.C. Harman, P.J. Taylor, M.P. Walsh, B.E. LaForge, Science 297 (2002) 2229.
[2] J.P. Heremans, V. Jovovic, E.S. Toberer, A. Saramat, K. Kurosaki, A. Charoenphakdee, S. Yamanaka, G.J. Snyder, Science 321 (2008) 554.
[3] a) R. Ionescu, J. Jaklovszky, N. Nistor, A. Chiculita, Phys. Stat. Sol. A 27 (1975) 27;
b) A.A. Joraide, J. Mater Sci. 30 (1995) 744;
c) Y. Lan, B. Poudel, Y. Ma, D. Wang, M.S. Dresselhaus, G. Chen, Z. Ren, Nano Lett. 9 (2009) 1419.
[4] D.J. Bergman, O. Levy, J. Appl. Phys. 70 (1991) 6821.
[5] D.J. Bergman, L.G. Fel, J. Appl. Phys. 85 (1999) 8205.
[6] M.G. Kanatzidis, Chem. Mater 22 (2010) 648.
[7] N. Gothard, G. Wilks, T.M. Tritt, J.E. Spowart, J. Electron. Mater 39 (2010) 1909.
[8] M. Popov, S. Buga, P. Vysikaylo, P. Stepanov, V. Skok, V. Medvedev, E. Tatyanin, V. Denisov, A. Kirichenko, V. Aksenenkov, V. Blank, Phys. Status Solidi A 208 (2011) 2783.
[9] V.D. Blank, S.G. Buga, V.A. Kulbachinskii, V.G. Kytin, V. V.Medvedev, M. Yu. Popov, P.B. Stepanov, V.F. Skok, Phys. Rev. B 86 (2012) 075426.
[10] X. Shi, L. Chen, J. Yang, G.P. Meisner, Appl. Phys. Lett. 84 (2004) 2301.
[11] X. Shi, L.D. Chen, S.Q. Bai, X.Y. Huang, X.Y. Zhao, Q. Yao, C. Uher, J. Appl. Phys. 102 (2007) 103709.
[12] Y. Zhang, X.L. Wang, W.K. Yeoh, R.K. Zeng, C. Zhang, Appl. Phys. Lett. 101 (2012) 031909.
[13] J. Seo, K. Park, D. Lee, C. Lee, Mater. Lett. 35 (1998) 4.
[14] D.Y. Chung, T. Hogan, P. Brazis, R.L. Melissa, Science 287 (2000) 1024.
[15] R. Venkatasubramanian, E. Siivola, T. Colpitts, B. O' Quinn, Nature 413 (2001) 597.
[16] W. Kim, J. Zide, A. Gossard, D. Klenov, S. Stemmer, A. Shakouri, A. Majumdar, Phys. Rev. Lett. 96 (2006) 045901.
[17] B. Poudel, Q. Hao, Y. Ma, Y.C. Chen, A. Minnich, B. Yu, X. Yan, D.Z. Wang, A. Muto, D. Vashaee, X.Y. Chen, J.M. Liu, M.S. Dresselhaus, G. Chen, Z.F. Ren, Science 320 (2008) 634.
[18] W.J. Xie, J. He, H.J. Kang, X.F. Tang, S. Zhu, M. Laver, S.Y. Wang, J.R.D. Copley, C.M. Brown, Q.J. Zhang, T.M. Tritt, Nano Lett. 10 (2010) 3283.
[19] C.J. Liu, H.C. Lai, Y.L. Liu, L.R. Chen, J. Mater. Chem. 22 (2012) 4825.
[20] Y.Y. Li, D. Li, X.Y. Qin, X.H. Yang, Y.F. Liu, J. Zhang, Y.C. Dou, C.J. Song, H.X. Xin, J. Mater. Chem. C 3 (2015) 7045–7052.
[21] M. Scheele, N. Oeschler, K. Meier, A. Kornowski, C. Klinke, H. Weller, Adv. Func. Mater 19 (2009) 3476.
[22] J. Kang, J.W. Roh, W. Shim, J. Ham, J.-S. Noh, W. Lee, Adv. Mater 23 (2011) 3414.
[23] Y.C. Zhang, H. Wang, S. Kraemer, Y.F. Shi, F. Zhang, M. Snedaker, K.L. Ding, M. Moskovits, G.J. Snyder, G.D. Stuck, ACS Nano 5 (2011) 3158.
[24] R.J. Mehta, Y.L. Zhang, C. Karthik, B. Singh, R.W. Siegel, T. Borca-Tasciuc, G. Ramanath, Nat. Mater 11 (2012) 233.
[25] J.S. Son, M.K. Choi, M.-K. Han, K. Park, J.-Y. Kim, S.J. Lim, M. Oh, Y. Kuk, C. Park, S.-J. Kim, T. Hyeon, Nano Lett. 12 (2012) 640.
[26] A. Soni, Z. Yanyuan, Y. Ligen, M.K.K. Aik, M.S. Dresselhaus, Q. Xiong, Nano Lett. 12 (2012) 1203.
[27] Y.C. Dou, X.Y. Qin, D. Li, Y.Y. Li, H.X. Xin, J. Zhang, Y.F. Liu, C.J. Song, L. Wang, RSC Adv. 5 (2015) 34251–34256.
[28] Y. Du, S.Z. Shen, W.D. Yang, R. Donelson, K.F. Cai, P.S. Casey, Synth. Met. 161 (2012) 2688–2692.
[29] A.C. Ferrari, J.C. Meyer, V. Scardaci, C. Casiraghi, M. Lazzeri, F. Mauri, S. Piscanec, D. Jiang, K.S. Novoselov, S. Roth, A.K. Geim, Phys. Rev. Lett. 97 (2006) 187401.
[30] D.H. Kim, C. Kim, S.H. Heo, H. Kim, Acta Mater 59 (2011) 405.
[31] J. Horak, K. Cermak, L. Koudelka, J. Phys. Chem. Solids 47 (1986) 805.
[32] S.N. Girard, J.Q. He, X.Y. Zhou, D. Shoemaker, C.M. Jaworski, C. Uher, V.P. Dravid, J.P. Heremans, M.G. Kanatzidis, J. Am. Chem. Soc. 133 (2011) 16588.
[33] K. Biswas, J.Q. He, Q.C. Zhang, G.Y. Wang, C. Uher, V.P. Dravid, M.G. Kanatzidis, Nat. Chem. (2011) 160.
[34] J. Zhou, X. Li, G. Chen, R. Yang, Phys. Rev. B Condens. Matter Mater. Phys. 82 (2010) 115308.
[35] J.Y.W. Seto, J. Appl. Phys. 46 (1975) 5247.
[36] J. Martin, L. Wang, L. Chen, G. Nolas, Phys. Rev. B Condens. Matter Mater. Phys. 79 (2009) 115311.
[37] E.S. Toberer, P. Rauwel, S. Gariel, J. Tao, G.J. Snyder, J. Mater. Chem. 20 (2010) 9877–9885.
[38] Y.B. Luo, J.Y. Yang, M. Liu, Y. Xiao, L.W. Fu, W.X. Li, D. Zhang, M.Y. Zhang, Y.D. Cheng, J. Mater. Chem. A 3 (2015) 1251.
[39] M.S. Dresselhaus, G. Chen, M.Y. Tang, R.G. Yang, H. Lee, D.Z. Wang, Z.F. Ren, J.P. Fleurial, P. Gogna, Adv. Mater 19 (2007) 1043–1053.
[40] B. Poudel, Q. Hao, Y. Ma, Science 320 (2008) 634.